THE JOURNAL OF BIOLOGICAL CHEMISTRY VOL. 284, NO. 45, pp. 31097–31108, November 6, 2009

A UV-responsive Internal Ribosome Entry Site Enhances Serine Hydroxymethyltransferase 1 Expression for DNA Damage Repair*

Received for publication, May 1, 2009, and in revised form, August 27, 2009 Published, JBC Papers in Press, September 4, 2009, DOI 10.1074/jbc.M109.015800

Jennifer T. Fox[‡], **William K. Shin**[§], **Marie A. Caudill**[§], **and Patrick J. Stover**[‡§1]

From the [‡]*Graduate Field of Biochemistry and Molecular and Cellular Biology and* [§]*Division of Nutritional Sciences, Cornell University, Ithaca, New York 14853*

Thymidine nucleotides are required for faithful DNA synthesis and repair, and their *de novo* biosynthesis is regulated by serine hydroxymethyltransferase 1 (SHMT1). The SHMT1 transcript contains a heavy chain ferritin, heterogeneous nuclear ribonucleoprotein H2, and CUG-binding protein 1-responsive internal ribosome entry site (IRES) that regulates SHMT1 translation. In this study a non-lethal dose of UVC is shown to increase SHMT1 IRES activity and protein levels in four different cell lines. The mechanism for the UV-induced activation of the SHMT1 IRES involves an increase in heavy chain ferritin and heterogeneous nuclear ribonucleoprotein H2 expression and the translocation of CUG-binding protein 1 from the nucleus to the cytoplasm. The UV-induced increase in SHMT1 translation is accompanied by an increase in the small ubiquitin-like modifier-dependent nuclear localization of the *de novo* thymidylate biosynthesis pathway and a decrease in DNA strand breaks, indicating a role for SHMT1 and nuclear folate metabolism in DNA repair.

UV radiation is mutagenic and damages cellular macromolecules, including proteins, lipids, and DNA. Thymine bases within DNA are sensitive to UV-induced damage, forming cyclobutane-type pyrimidine dimers and (6–4)-photoproducts (1). These lesions hinder RNA polymerase processivity and, thus, inhibit transcription (2). In mammalian cells, cyclobutane-type pyrimidine dimers and (6–4)-photoproducts are repaired by nucleotide excision repair (NER).[2] NER involves the removal of ~30 nucleotides surrounding the damage site, resulting in a single-strand gap that requires DNA synthesis and ligation to complete the repair process (3).

Thymidine triphosphate is required for faithful DNA synthesis. Insufficient pools of thymidine nucleotides during DNA replication and NER result in elevated rates of uracil misincorporation into DNA, which ultimately leads to DNA strand breaks and genome instability (4). Thymidine nucleotides can either be synthesized through a salvage pathway or can be synthesized *de novo* through folate-mediated one-carbon metabolism (see Fig. 1). In the *de novo* biosynthetic pathway, 5,10-methylenetetrahydrofolate (5,10-methylene-THF) provides the activated one-carbon units and reducing equivalents for the thymidylate synthase (TS)-catalyzed conversion of deoxyuridine monophosphate (dUMP) to thymidylate. 5,10-Methylene-THF can be generated by two alternative pathways; that is, the reduction of 10-formyl-THF or through the activity of serine hydroxymethyltransferase 1 (SHMT1), which catalyzes the conversion of THF and serine to glycine and 5,10-methylene-THF.

The SHMT1 enzyme is a key regulator of *de novo* thymidylate biosynthesis and is poised to play a role in the repair of UV-induced DNA damage. In addition to providing 1-carbon units for the synthesis of thymidylate, SHMT1-derived 5,10-methylene-THF can be reduced by methylene-THF reductase to form 5-methyl-THF, a cofactor utilized in the remethylation of homocysteine to methionine (see Fig. 1). The concentration of free folate in the cell is negligible, and therefore, TS and methylene-THFR compete for limiting pools of the 5,10-methylene-THF cofactor (5–8). Several studies have demonstrated that whereas the majority of 5,10-methylene-THF derived from the reduction of 10-formyl-THF is directed toward the synthesis of methionine (9, 10), SHMT1-derived 5,10-methylene-THF is partitioned to TS (11) through the cell cycle-dependent and small ubiquitin-like modifier (SUMO)-mediated nuclear localization of the thymidylate biosynthesis pathway (12, 13) that enables the nuclear *de novo* synthesis of thymidylate (14) (Fig. 1).

The DNA damage caused by UV radiation evokes adaptive cellular responses which include cell cycle arrest (15) and changes in transcription (16, 17) and translation. At the translational level, UV radiation reduces global cap-dependent protein synthesis by inducing the phosphorylation of eukaryotic initiation factor 2α (eIF2α) (18–20) and thereby preventing the recycling of the ternary complex (eIF2·GTP·$tRNA_b^{Met}$) (21). Despite the reduction in cap-dependent translation, several mRNAs whose protein products are essential for the UV-induced stress response (for example, p53 (22) and Apaf-1 (23)) have evolved alternative mechanisms of protein synthesis that allow for their continued expression after exposure to UV. One

* This work was supported, in whole or in part, by National Institutes of Health Grant DK58144 from the USPHS.

[1] To whom correspondence should be addressed: Cornell University, 315 Savage Hall, Ithaca NY 14853. Tel.: 607-255-8001; Fax: 607-255-9751; E-mail: pjs13@cornell.edu.

[2] The abbreviations used are: NER, nucleotide excision repair; SHMT1, serine hydroxymethyltransferase 1; UTR, untranslated region; IRES, internal ribosome entry site; H ferritin, heavy chain ferritin; hnRNP H2, heterogeneous nuclear ribonucleoprotein H2; CUGBP1, CUG-binding protein 1; THF, tetrahydrofolate; TS, thymidylate synthase; MCF-7, mammary adenocarcinoma; eIF2α, eukaryotic initiation factor 2α; SUMO, small ubiquitin-like modifier; Rluc, Renilla luciferase; Fluc, Firefly luciferase; siRNA, small interference RNA; α-MEM, minimum Eagle's medium; MTT, thiazolyl blue tetrazolium bromide; GAPDH, glyceraldehyde-3-phosphate dehydrogenase.

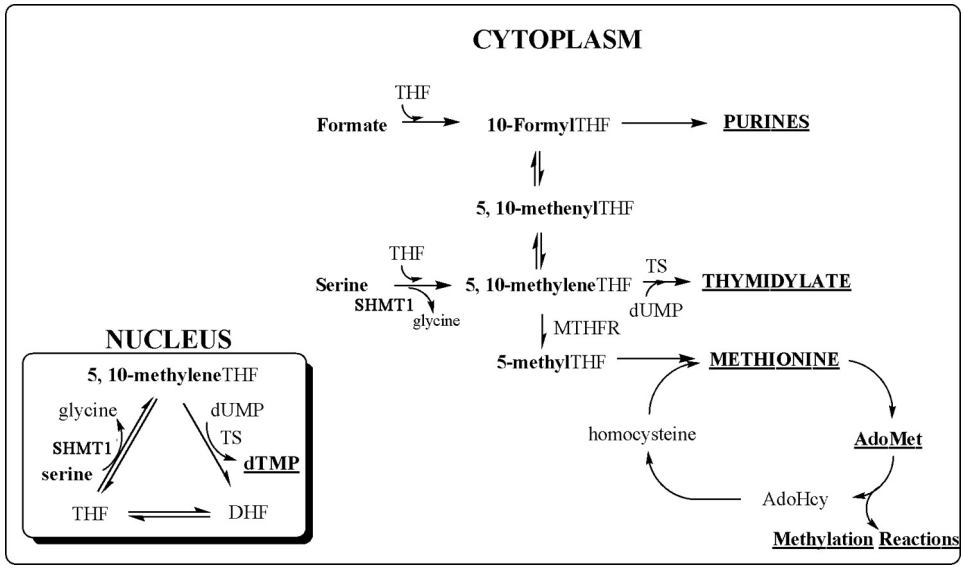

FIGURE 1. **Folate-mediated one-carbon metabolism.** Folate-mediated one-carbon metabolism is required for the *de novo* synthesis of purines and thymidylate and for the remethylation of homocysteine to methionine. Mitochondrial-derived formate can enter the cytoplasm and function as a one-carbon donor through the conversion of THF to 10-formyl-THF. 5,10-Methylene-THF, which can be generated through the reduction of 10-formyl-THF or through the catalytic activity of SHMT1, provides the one-carbon units for the TS-catalyzed conversion of dUMP to thymidylate. It also serves as a substrate for methylene-THF reductase (*MTHFR*), which reduces 5,10-methylene-THF to ultimately form *S*-adenosylmethionine (*AdoMet*), the one-carbon donor in numerous cellular methylation reactions. *De novo* thymidylate biosynthesis also occurs in the nucleus through the SUMO-dependent import of the thymidylate synthesis pathway during S-phase. *Hcy*, homocysteine; *DHF*, dihydrofolate.

such mechanism involves ribosome recruitment to an internal ribosome entry site (IRES) located within the 5′-untranslated region (UTR) of the transcript (24, 25).

We have previously shown that the SHMT1 5′-UTR contains an IRES whose activity is stimulated by heavy chain ferritin (H ferritin), heterogeneous nuclear ribonucleoprotein H2 (hnRNP H2) (55), and CUG-binding protein 1 (CUGBP1) (26). However, the responsiveness of the IRES to stress stimuli that inhibit cap-dependent translation has not been explored. In the present study we demonstrate the role of the SHMT1 IRES- and SUMO-mediated nuclear translocation of the folate-dependent nuclear thymidylate biosynthesis in UV-induced DNA damage repair.

EXPERIMENTAL PROCEDURES

Cell Culture—Human MCF-7 mammary adenocarcinoma cells (HTB22), HeLa cells (CCL2), and pagetoid sarcoma skin fibroblasts (CRL-7677) were obtained from ATCC. The human SH-SY5Y neuroblastoma, a subline of the SK-N-SH neuroblastoma, was obtained from June Biedler (Fordham University). MCF-7, HeLa, and SH-SY5Y cells were cultured in α-MEM (Hyclone Laboratories) containing 11% fetal bovine serum (Hyclone Laboratories). Pagetoid sarcoma skin fibroblasts were cultured in Dulbecco's modified Eagle's medium (Invitrogen) containing 11% fetal bovine serum (Hyclone Laboratories). All cells were maintained at 37 °C and 5% CO_2.

Treatment and Preparation of Cell Extracts—MCF-7 cells at 30% confluence were arrested at the G_2/M phase of the cell cycle by treatment with 60 ng/ml nocodazole (Calbiochem) for 24 h. Cell cycle analysis was carried out by fluorescence-activated cell sorting using 3 mM sodium citrate containing 1% Triton X-100 and 50 ng/ml propidium iodide as the lysis/DNA binding reagent. For experiments involving UV treatment, cells at 95% confluence were washed twice with phosphate-buffered saline and then exposed to 10,000 μJ/cm^2 UV (254 nm) using the Stratagene UV Stratalinker 2400. The medium was then replaced, and the cells were cultured under normal conditions. At the indicated time intervals after treatment, the cells were harvested by trypsinization and washed in phosphate-buffered saline. To obtain whole cell extracts, the cells were resuspended in lysis buffer (50 mM Tris, pH 7.5, 150 mM NaCl, 1% Nonidet P-40, 5 mM EDTA, 1 mM phenylmethylsulfonyl fluoride, 1:100 dilution of Sigma protease inhibitor mixture, 10 mM *N*-ethylmaleimide) and lysed on ice for 30 min. Nuclear and cytoplasmic extracts were obtained using the NE-PER nuclear and cytoplasmic extraction kit (Pierce) according to the manufacturer's protocol. The protein concentration of all extracts was determined using the Lowry assay as modified by Bensadoun and Weinstein (27).

Trypan Blue Exclusion—MCF-7 cells were treated with UV according to the protocol above. 24 h after UV exposure the cells were harvested by trypsinization, pelleted by centrifugation, and then resuspended in serum-free α-MEM. The suspension was then diluted 1:1 with 0.4% trypan blue (Invitrogen), and the viable and non-viable cells were counted using a hemocytometer.

Metabolic Labeling—Control and UV-irradiated cells were labeled with 100 μCi/ml EasyTag^{TM} Expre^{35}S^{35}S protein labeling mix (PerkinElmer Life Sciences, 1175 Ci/mmol) for 30 min in methionine/cysteine-free Dulbecco's modified Eagle's medium (Sigma). Cells were then harvested and lysed as described above. The protein concentration of all extracts was determined using the Lowry assay as modified by Bensadoun and Weinstein (27), and equal amounts of extract were separated by 12% SDS-PAGE. The gel was stained with Coomassie Blue (R-250), dried, and autoradiographed. To quantify the amount of ^{35}S incorporation, equal amounts of protein were precipitated with trichloroacetic acid, and radioactivity was quantified in a LS 6500 multipurpose scintillation counter (Beckman Coulter).

Western Blotting—Proteins were separated by SDS-PAGE using a Tris-glycine gel and transferred to a polyvinylidene difluoride membrane. The membrane was blocked with 5% nonfat dry milk in phosphate-buffered saline containing 1% Nonidet P-40 for 1 h at room temperature, incubated with primary antibody overnight at 4 °C, and then incubated with horseradish peroxidase-conjugated anti-IgG for 1–3 h at room

temperature. After each incubation, the membrane was washed with phosphate-buffered saline, 0.1% Tween 20. Proteins were visualized using Super Signal® substrate (Pierce) followed by autoradiography. Mouse anti-phospho-p53 (Ser-15, Cell Signaling) was used at a 1:1000 dilution, rabbit anti-phospho-eIF2α (Ser51, Cell Signaling) was used at a 1:1,000 dilution, affinity-purified sheep anti-human SHMT1 was used at a 1:40,000 dilution, sheep anti-TS (Abcam) was used at a 1:2,000 dilution, mouse anti-CUGBP1 (3B1, Santa Cruz Biotechnology) was used at a 1:10,000 dilution, affinity-purified sheep anti-H ferritin was used at a 1:500 dilution, goat anti-hnRNP H (N-16, Santa Cruz Biotechnology) was used at a 1:1,000 dilution, rabbit anti-SUMO-1 (Active Motif) was used at a 1:1,000 dilution, rabbit anti-p53 (Active Motif) was used at a 1:1,000 dilution, goat anti-eIF2α (Santa Cruz Biotechnology) was used at a 1:1,000 dilution, rabbit anti-Lamin A (H-102, Santa Cruz Biotechnology) was used at a 1:1,000 dilution, and mouse anti-GAPDH (Novus Biologicals) was used at a 1:40,000 dilution. Goat anti-mouse IgG, rabbit anti-sheep IgG, rabbit anti-goat IgG, and goat anti-rabbit IgG were all purchased from Pierce and used at a 1:5000 dilution. When necessary, membranes were stripped with 0.2 M sodium hydroxide.

Real Time PCR—RNA was extracted from cells using Trizol (Invitrogen) according to the manufacturer's protocol. After incubating with DNase I for 1 h at 37 °C to remove any residual DNA, the RNA was purified using the RNeasy mini kit (Qiagen) and reverse-transcribed into cDNA using the High Capacity cDNA reverse transcription kit (Applied Biosystems). The PCR was carried out using either the 2× Taqman Universal PCR mix and 6-carboxyfluorescein-labeled Taqman probes complimentary to SHMT1 (Hs00541038_m1) and GAPDH (Hs99999905_m1) or the QuantiFast SYBR Green PCR kit (Qiagen) and primers complimentary to Fluc (5′-ATTTATCGGAGTTGCAGTTGCGCC-3′; 5′-GCTGCGAAATGCCCATACTGTTGA-3′) and Rluc (5′-AACGCGGCCTCTTCTTATTT-3′; 5′-ATTTGCCTGATTTGCCCATA-3′). PCR products were quantified using the Applied Biosystems 7500 real time PCR System.

Polysome Profile Analysis—MCF-7 cells at ~80% confluence were treated with UVC following the protocol above. 22 h after UV exposure the cells were treated with 50 μg/ml cycloheximide (Sigma) for 30 min at 37 °C and 5% CO_2. The cells were scraped from the plate and then lysed in polysome extraction buffer (10 mM Tris, pH 7.5, 10 mM NaCl, 1.5 mM $MgCl_2$, 1% Triton X-100, 1% deoxycholate, 2% Tween 20, 1000 units of recombinant RNasin® ribonuclease Inhibitor (Promega)) for 10 min on ice. Nuclei were pelleted by brief centrifugation, and the resulting supernatant was fractionated through a 10–50% sucrose gradient by ultracentrifugation in a SW41-Ti rotor for 2 h at 36,000 rpm and 4 °C. 1-ml fractions were collected with a density gradient fractionation system (Brandel), and the absorbance at 254 nm was measured continuously as a function of gradient depth. RNA was isolated by phenol-chloroform extraction, treated with DNase I for 1 h at 37 °C and then reverse-transcribed using the SuperScript III First-Strand Synthesis System (Invitrogen) according to the manufacturer's protocol. The PCR was carried out using primers specific to SHMT1 (5′-ATGCCCTACAAGGTGAACCCAGAT-3′ (forward) and 5′-ACCACATGGCAGTGTTCAAATGGG-3′ (reverse)), CUGBP1 (5′-TCACTTGGAGCCCTGCAGACATTA-3′ (forward) and 5′-AGCAGCATATTGCTGGATACCCGA-3′ (reverse)), and ATF4 (5′-CCAACAACAGCAAGGAGGATGCCTTCTC-3′ (forward) and 5′-GGATCATGGCAACGTAAGCAGTGTAGTC-3′ (reverse)).

Generation of Capped Bicistronic mRNA for Use in MCF-7 Cell Transfections—The generation of pSP64 poly(A) DNA templates containing the Renilla and Firefly luciferase reporter genes and either the SHMT1 5′-UTR, SHMT1 5′-UTR, and 3′-UTR, the reverse complement of the SHMT1 5′-UTR (reverse UTR), or the mouse SHMT1 5′-UTR is described elsewhere (26). The DNA templates were linearized with EcoRI and purified using the Roche Applied Science PCR clean-up column. The templates were transcribed using the T7 mMESSAGE mMACHINE kit (Ambion) according to the manufacturer's protocol. The crude mRNA was treated with DNase I (Ambion) for 15 min at 40 °C and precipitated in 2 M LiCl at −80 °C. All RNA procedures were conducted under RNase-free conditions, and all mRNA was stored with Recombinant RNasin® ribonuclease inhibitor (Promega). The mRNA was quantified by spectrophotometry, and its quality was verified by electrophoresis.

mRNA Transfections—Cells were cultured in 6-well plates and then treated with UVC or nocodazole according to the protocol above. 12 h after UV treatment or 24 h after nocodazole treatment, the cells were incubated in Opti-MEM (Invitrogen) containing a 1:100 dilution of DMRIE-C transfection reagent (Invitrogen) and 5 μg/ml bicistronic mRNA (capped and polyadenylated) for 4 h at 37 °C and 5% CO_2. The Opti-MEM was then replaced with α-MEM or Dulbecco's modified Eagle's medium, and the cells were incubated for an additional 6 h at 37 °C and 5% CO_2. Renilla and Firefly Luciferase activity was quantified on a Veritas Microplate Luminometer (Turner Biosystems) using the Dual-Glo luciferase assay system (Promega) according to the manufacturer's protocol.

siRNA Transfections—MCF-7 cells were grown to ~40% confluence in 6-well plates. The cells were transfected with 5 nM concentrations of either negative control siRNA (Ambion), hnRNP H2 siRNA (Qiagen; r(CAU GAG AGU ACA UAU UGA A)dTdT (sense) and r(UUC AAU AUG UAC UCU CAU G)dGdG (antisense)), or CUGBP1 siRNA (Qiagen; r(GGAACUCUUCGAACAGUAU)dTdT (sense) and r(AUACUGUUCGAAGAGUUCC)dCdG (antisense)) using the HiPerFect transfection reagent (Qiagen) according to the manufacturer's instructions. After incubation with siRNA for 48 h at 37 °C and 5% CO_2, the cells were treated with UVC according to the protocol above. The cells were then either lysed and subjected to SDS-PAGE/immunoblot analysis to determine knockdown efficiency or used in mRNA transfection experiments as described above.

Immunofluorescence—MCF-7 cells were grown on sterile coverslips to ~30% confluence and then exposed to 10,000 μJ/cm^2 UV (254 nm) according to the protocol above. 22 h after UV treatment, the coverslips were incubated in phosphate-buffered saline containing 10 μM DRAQ5 (Biostatus Ltd.) for 5 min at room temperature and then fixed with 100% methanol for 5 min. After a brief wash in phosphate-buffered saline, the

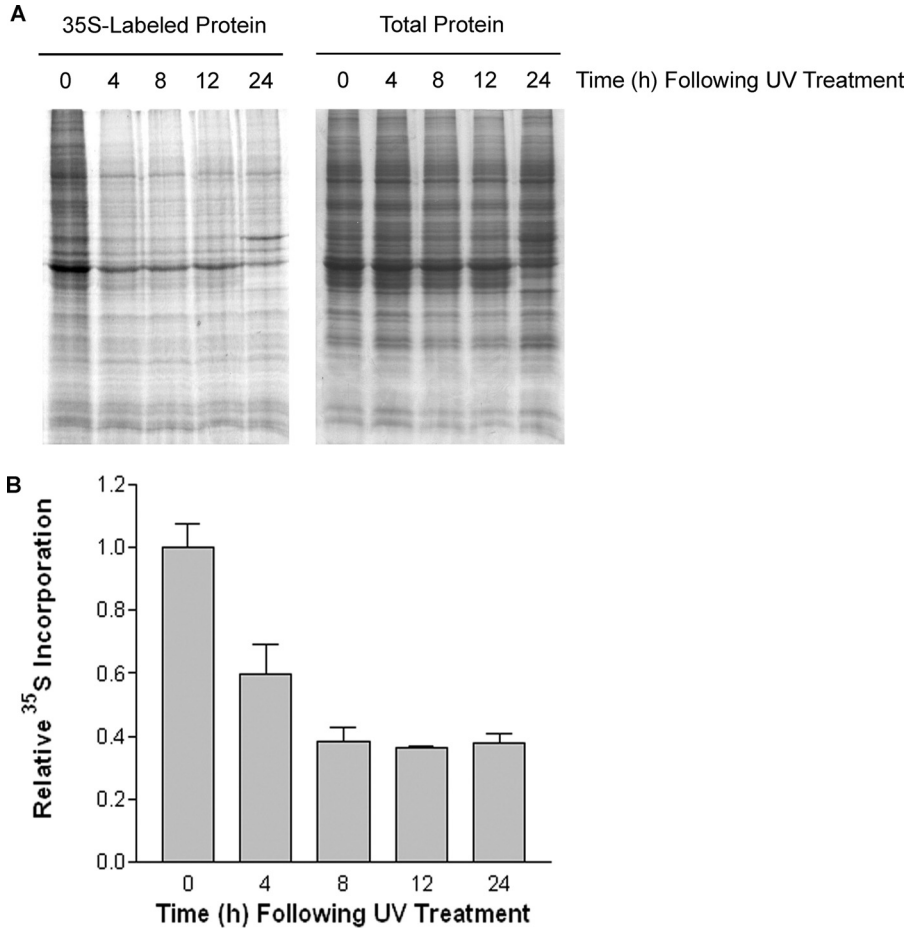

FIGURE 2. **Nascent protein synthesis decreases after UV treatment.** *A*, MCF-7 cells were treated with 10,000 μJ/cm^2 UVC (254 nm). At the indicated times after UV treatment, the cells were pulse-labeled with [^{35}S]Met/Cys, and total cell extracts were resolved by SDS-PAGE. The gel was then stained with Coomassie Blue (*right panel*) to visualize total proteins followed by autoradiography (*left panel*) to detect newly synthesized proteins. *B*, equal amounts of protein from *A* were precipitated with trichloroacetic acid, and ^{35}S incorporation was quantified in a scintillation counter. The counts per min recorded for the 0 h sample was given a value of 1.0. The data represent the average of three independent trichloroacetic acid precipitations ±S.E.

coverslips were blocked with phosphate-buffered saline containing 2% bovine serum albumen and 0.1% Triton X-100. After 2 h the blocking solution was removed, and the coverslips were incubated in phosphate-buffered saline containing 2% bovine serum albumen and a 1:250 dilution of mouse anti-CUGBP1 (3B1, Santa Cruz Biotechnology) for 2 h at room temperature. After extensive washing with phosphate-buffered saline, the coverslips were incubated in phosphate-buffered saline containing 2% bovine serum albumen and a 1:500 dilution of an Alexa-Fluor 488-conjugated goat anti-mouse IgG secondary antibody (Invitrogen) for 1 h. The coverslips were then washed extensively with phosphate-buffered saline and mounted to slides using Fluoromount-G (Southern Biotech). The cells were visualized using a Leica TCS SP2 confocal microscope at the Cornell University Microscopy and Imaging Facility.

Comet Assay—MCF-7 cells were grown to ~20% confluence in 6-well plates. The cells were transfected with 5 nM concentrations of either negative control siRNA (Ambion) or SHMT1 siRNA (Qiagen; r(CUAGGCUCUUGCUUAAAUA)dTdT (sense) and r(UAUUUAAGCAAGAGCCUAG)dGdG (antisense)) using the HiPerFect transfection reagent (Qiagen) according to the manufacturer's instructions. After incubation with siRNA for 55 h at 37 °C and 5% CO_2, the cells were exposed to 10,000 μJ/cm^2 UV (254 nm) according to the protocol above. At the indicated times after UV treatment, the cells were scraped from the plate. Half of the cells were subjected to Western blot analysis according to the protocol above to confirm SHMT1 knockdown. The other half were resuspended in α-MEM (Hyclone Laboratories) supplemented with 10% DMSO and 20 mM EDTA, pH 7.5, dispensed into cryogenic tubes, frozen in liquid nitrogen, and stored at −80 °C.

The cryopreserved cells from above were thawed at room temperature and then diluted to a final concentration of 10^5 cells/ml with phosphate-buffered saline, pH 7.4. The diluted cells were then combined 1:10 with 1% low melting point agarose and dispensed onto a CometSlide (Trevigen). After the agarose solidified, the slides were immersed in lysis solution (10% DMSO, 1% Triton X-100, 2.5 M NaCl, 100 mM EDTA, 10 mM Tris, pH 10.2) for 1–3 h at 4 °C. After a 10-min incubation in 0.4 M Tris, pH 7.5, the slides were placed in an electrophoresis tank and incubated in alkaline (pH 13) electrophoresis buffer (0.3 M NaOH, 1 mM EDTA, pH 8.0) for 20 min at 4 °C to allow for the unwinding of supercoiled DNA. Electrophoresis was carried out at 27 V for 40 min at 4 °C. The slides were then incubated in 0.4 M Tris, pH 7.5, for 15 min, washed for 5 min in 100% ethanol, and dried overnight. To assess DNA damage, the dried slides were flooded with SYBR Gold™ (Invitrogen) and then visualized at 20× magnification using a fluorescent microscope (Olympus BX-50) at the Cornell University Microscopy and Imaging Facility. Cells were photographed using a QImaging Retiga EXi cooled CCD camera and analyzed using Komet 5.5 software (Andor Technology). The parameters analyzed included % tail DNA (the proportion of DNA that has migrated from the nucleoid core), tail length (the distance (microns) of DNA migration from the nucleoid core), extent tail moment (% tail DNA × tail length/100), and olive tail moment ((tail center of gravity − head center of gravity) × % tail DNA/100). The olive tail moment value captures both the smallest detectable size of migrating DNA (which is quantified in the comet tail length) and the number of strand breaks (quantified by the intensity of DNA in the tail). The mean value from 75 scored cells was taken as an index of damage for a given sample. Sensitivity of the assay was established by incubating untreated MCF-7 cells in 0, 50, 100, or 200 μM hydrogen peroxide for 15 min before lysis and then quantifying the

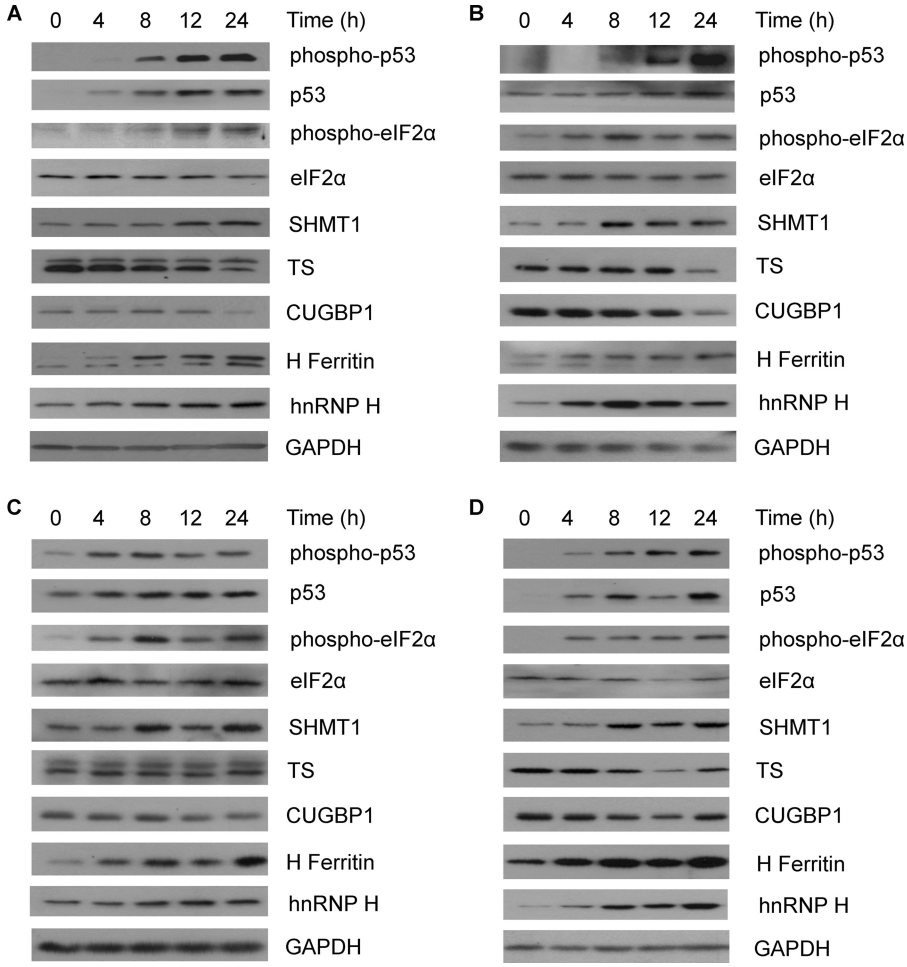

FIGURE 3. **Effect of UVC on protein levels.** MCF-7 cells (*A*), HeLa cells (*B*), transformed skin fibroblasts (*C*), and SH-SY5Y cells (*D*) were treated with 10,000 μJ/cm^2 UVC (254 nm). At the indicated times after UV treatment, total protein lysates were prepared and resolved by SDS-PAGE. Protein levels were determined by immunoblotting using antibodies against phosphorylated p53, p53, phosphorylated eIF2α, eIF2α, SHMT1, TS, CUGBP1, H ferritin, and hnRNP H. GAPDH served as a control for equal protein loading.

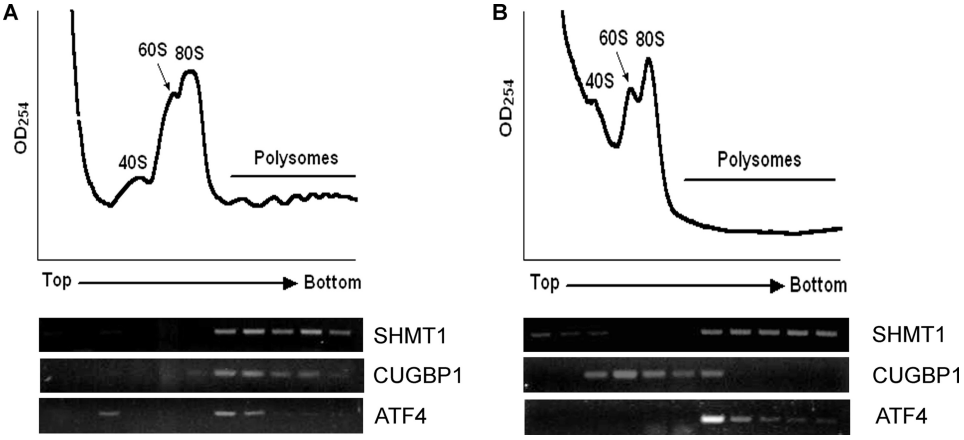

FIGURE 4. **SHMT1 mRNA remains associated with polysomes after UV exposure.** The polysome profile of untreated (*A*) and UV-irradiated MCF-7 cells (*B*) was recorded 22 h after UV treatment. The ribosomal species, as determined by the optical density (*OD*) at 254 nm, are indicated. Total RNA was extracted from each fraction, and SHMT1 mRNA was detected by reverse transcription PCR. CUGBP1 mRNA, which is not known to contain an IRES, and ATF4 mRNA, which is known to be translated during conditions where cap-dependent translation is reduced by the phosphorylation of eIF2α (52–54), are shown for comparison.

resulting comets as stated above. The concordance of each measured parameter in relation to hydrogen peroxide concentration (R^2) ranged from 0.92 to 0.96.

Thiazolyl Blue Tetrazolium Bromide (MTT) Assay—MCF-7 cells were treated with either negative control siRNA or SHMT1 siRNA and then exposed to 10,000 μJ/cm^2 UVC according to the protocol above. 24 h after UV treatment, MTT (Sigma) was added to the medium (final concentration of MTT, 0.5 mg/ml). After a 1-h incubation at 37 °C, 5% CO_2, the media were removed from the cells, and the insoluble formazan (formed by the reduction of MTT by living mitochondria) was resuspended in DMSO. The absorbance at 550 nm was measured using a Dynex MRXTC II microplate reader.

Immunoprecipitations—MCF-7 whole cell extracts were incubated for 2 h at 4 °C with 40 μl of protein A/G-conjugated agarose beads (Pierce) to remove nonspecific matrix-binding proteins. The precleared extracts were incubated with 10 μg of either sheep IgG (Pierce), affinity-purified sheep anti-human SHMT1 antibody, or sheep-anti-human TS antibody (Abcam) overnight at 4 °C. 40 μl of the protein A/G-agarose beads were then added, and the reaction was allowed to incubate for 2 h at 4 °C. The beads were collected and washed 5 times with lysis buffer (50 mM Tris, pH 7.5, 150 mM NaCl, 1% Nonidet P-40, 5 mM EDTA, 1 mM phenylmethylsulfonyl fluoride, 1:100 dilution of Sigma protease inhibitor mixture), and bound proteins were eluted in 2× SDS-PAGE sample buffer (160 mM Tris, pH 6.8, 20 mM dithiothreitol, 4% SDS, 20% glycerol) at 95 °C for 10 min. The samples were analyzed by Western blotting as described above, except that TrueBlot™ (eBioscience, 1:1000 dilution) was used as the secondary antibody to eliminate IgG contamination.

RESULTS

The Expression of SHMT1 Is Induced by UV Radiation—Previously we showed that SHMT1 is rate-limiting for *de novo* thymidylate biosynthesis during DNA replication in MCF-7 cells (28) and that mice lacking SHMT1 exhibit elevated levels of uracil in nuclear DNA (29). In this study the effect of UV radiation on

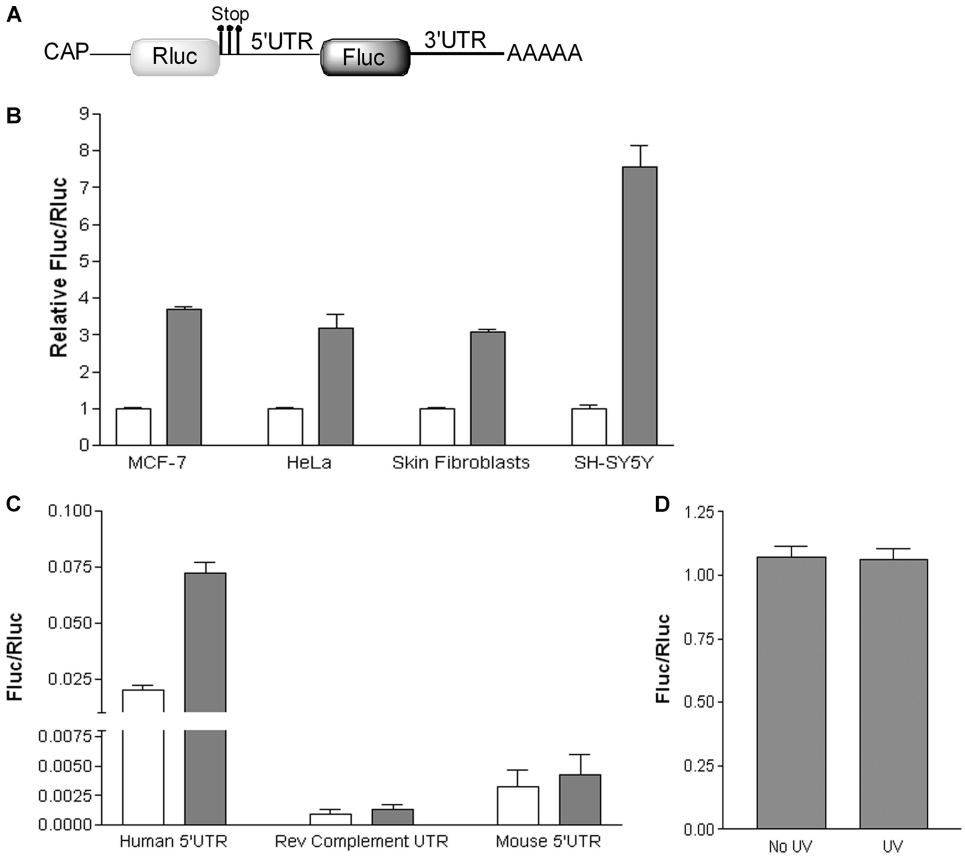

FIGURE 5. **UV treatment results in an increase in SHMT1 IRES activity.** *A*, shown is the bicistronic construct used to quantify SHMT1 IRES activity. It consists of (in the 5′ to 3′ direction) a cap analog, the Rluc reporter gene followed by three sequential in-frame stop codons, the human SHMT1 5′-UTR, which contains the IRES element, the Fluc reporter gene, the human SHMT1 3′-UTR, which was shown to stimulate SHMT1 IRES activity (26), and a 30-nucleotide poly(A) tail. *B*, untreated (*light bars*) and UV-treated (*dark bars*) cells were transiently transfected with the bicistronic construct in *A*. 22 h after treatment Fluc and Rluc activities were quantified. The relative ratio of total Fluc activity divided by total Rluc activity in untreated cells was given a value of 1.0. The data represent the average of three independent experiments ±S.E. *C*, untreated (*light bars*) and UV-treated (*dark bars*) MCF-7 cells were transiently transfected with either the bicistronic construct containing the human SHMT1 5′-UTR or bicistronic constructs where the human SHMT1 5′-UTR was replaced with either the reverse (*Rev*) complement of the human SHMT1 5′-UTR or the mouse SHMT1 5′-UTR. None of the bicistronic constructs used in this experiment contained the SHMT1 3′-UTR. IRES activity is reported as the ratio of total Fluc activity divided by total Rluc activity as measured 22 h after UV treatment. The data represent the average of three independent experiments ±S.E. *D*, MCF-7 cells were treated with 10,000 μJ/cm^2 UVC and transiently transfected with the bicistronic mRNA in *A*. 22 h after UV treatment, total RNA was extracted from the cells and reverse-transcribed into cDNA. Rluc and Fluc mRNA levels were determined by real time PCR. The data represent the average of three independent experiments ±S.E.

SHMT1 protein levels was examined to investigate the regulation of the enzymes in the nuclear thymidylate biosynthesis pathway during DNA repair. MCF-7 cells were treated with 10,000 μJ/cm^2 UVC (254 nm). This dose of UV was not lethal, as 90% of treated cells remained viable 24 h after UV exposure compared with 97% of untreated cells. However, the dose was sufficient to evoke a stress response. As anticipated based on previous studies (18–20, 30), global protein synthesis was impaired (Fig. 2, *A* and *B*), p53 protein levels increased (Fig. 3*A*), and both p53 and eIF2α became phosphorylated in a time-dependent manner after UV exposure (Fig. 3*A*), indicating that DNA damage had occurred and that cap-dependent protein synthesis was reduced. Western blot analysis of SHMT1 protein levels revealed that despite the decrease in cap-dependent translation, SHMT1 protein levels were increased 12 and 24 h after UV treatment (Fig. 3*A*). The increase in SHMT1 protein levels in response to UV exposure was not specific to MCF-7 cells, as similar results were obtained with cervical cancer (HeLa) cells (Fig. 3*B*), transformed skin fibroblasts (Fig. 3*C*), and neuroblastoma (SH-SY5Y) cells (Fig. 3*D*).

The SHMT1 IRES Is UV-responsive—SHMT1 mRNA levels did not increase after UV treatment, indicating that the increase in SHMT1 protein levels may be because of elevated rates of translation. Consistent with this hypothesis, the polysome analysis of untreated (Fig. 4*A*) and UV-treated (Fig. 4*B*) MCF-7 cells revealed that SHMT1 mRNA continued to be actively translated after UV exposure. CUGBP1 mRNA, which is not known to contain IRES activity, was not associated with polysomes after UV exposure (Fig. 4*B*). ATF4 mRNA, whose translation increases when cap-dependent translation is reduced after the phosphorylation of eIF2α (51–53), is present in the polysomes after UV exposure (Fig. 4*B*). Because cellular IRESs are typically responsive to stress stimuli that inhibit global cap-dependent translation (24), the effect of UV treatment on SHMT1 IRES activity was investigated. After UV treatment, MCF-7 cells, HeLa cells, transformed skin fibroblasts, and SH-SY5Y cells were transfected with bicistronic mRNAs. The biscistronic transcript contained the SHMT1 5′-UTR inserted between the Renilla luciferase (Rluc) and Firefly luciferase (Fluc) reporter genes and the SHMT1 3′-UTR located 3′ of the Fluc gene (Fig. 5*A*). Whereas expression of the first cistron in this transcript (Rluc) is cap-dependent, expression of the second cistron (Fluc) is dependent on IRES activity. The activity of the SHMT1 IRES increased significantly in all UV-exposed cells compared with unexposed cells as quantified by the Fluc/Rluc ratio (Fig. 5*B*). Bicistronic mRNAs containing either the reverse complement of the SHMT1 5′-UTR or the mouse SHMT1 5′-UTR, both of which have been shown previously to lack IRES activity (26), were not stimulated by UV exposure (Fig. 5*C*). The results from these control bicistronic mRNAs demonstrate that SHMT1 IRES activity is associated only with the human 5′-UTR and indicate that ribosomal re-initiation cannot account for the induction of Fluc translation after UV exposure. Real time PCR analysis of Fluc and Rluc RNA levels after the transfections revealed that degradation of the bicistronic construct is likewise not respon-

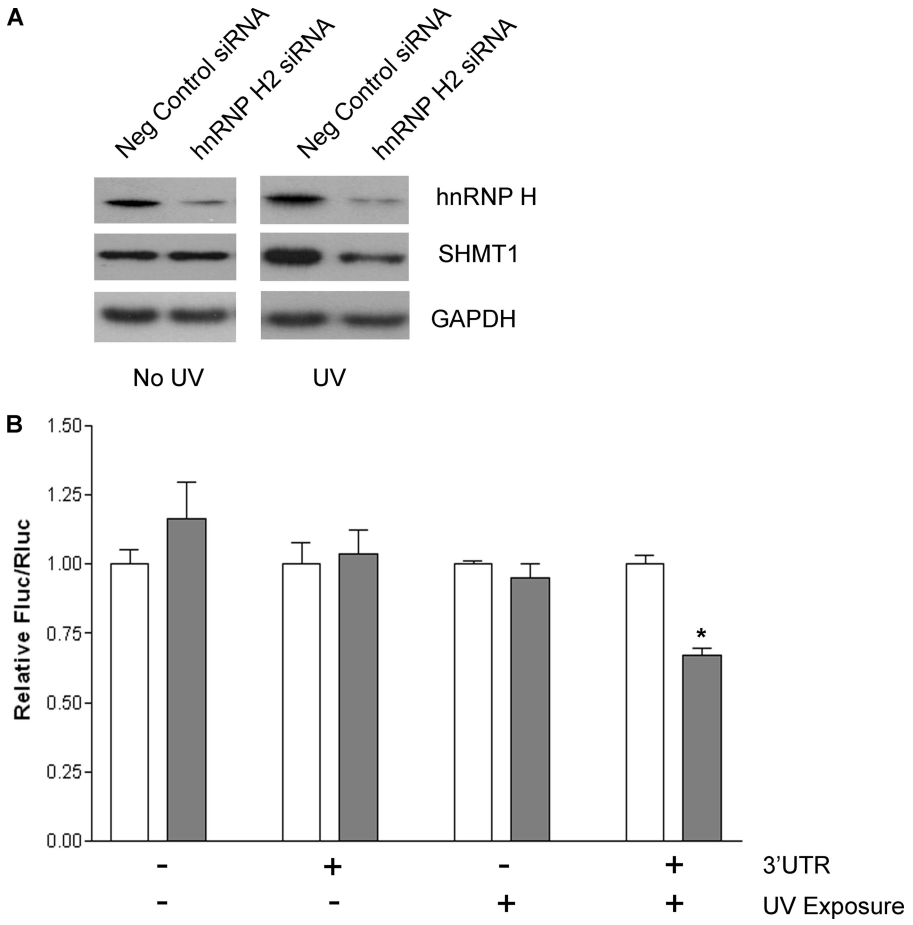

FIGURE 6. **hnRNP H2 is involved in the UV-induced activation of the SHMT1 IRES.** *A*, MCF-7 cells were transfected with negative control siRNA or hnRNP H2 siRNA, treated with UV, and then subjected to Western blot analysis using antibodies against hnRNP H and SHMT1. GAPDH serves as a control for equal protein loading. *B*, control (*white bars*) and hnRNP H2 siRNA-treated cells (*dark bars*) were transiently transfected with bicistronic mRNAs with and without the SHMT1 3′-UTR and in the presence and absence of UVC exposure. The relative ratio of Fluc/Rluc for each bicistronic mRNA in the control cells was given a value of 1.0. The data represent the average of three independent experiments ±S.E. The *asterisk* represents statistical significance ($p = 0.001$) as determined by Student's *t* test.

sible for the increase in the Fluc/Rluc ratio after UV treatment (Fig. 5*D*).

The UV-induced Increase in SHMT1 IRES Activity Is Mediated by H Ferritin, hnRNP H2, and CUGBP1—SHMT1 IRES activity has previously been shown to be stimulated by H ferritin (26) and the IRES *trans*-acting factors hnRNP H2 and CUGBP1 (26, 55). It is known that the regulation of many cellular IRESs during stress conditions depends on a change in concentration and/or subcellular location of IRES *trans*-acting factors. For example, during apoptosis, an increase in polypyrimidine tract binding protein levels correlates with the activity of apoptotic IRESs (31); the genotoxic- stress-induced IRES-mediated translation of BAG-1 results from the relocalization of the BAG-1 IRES *trans*-acting factors from the nucleus to the cytoplasm (32), and the relocalization of hnRNPA1 from the nucleus to the cytoplasm after osmotic shock inhibits XIAP IRES activity (33). Thus, given the significant role that H ferritin, hnRNP H2, and CUGBP1 play in the stimulation of SHMT1 IRES activity, their concentration and/or subcellular localization after UV treatment was investigated.

Several transcription factors are activated by UV-induced DNA damage. Among them is NFκB (34), a known activator of H ferritin expression (35). In agreement with the UV-induced activation of NFκB, Western blot analysis of H ferritin protein levels in MCF-7 cells, HeLa cells, transformed skin fibroblasts, and SH-SY5Y cells revealed a time-dependent increase after UV treatment (Fig. 3, *A–D*).

Western blot analysis of hnRNP H1/H2 protein levels in all four cell lines also revealed a time-dependent increase after UV treatment (Fig. 3, *A–D*). To determine whether hnRNP H2 is essential for SHMT1 IRES activation by UV, siRNA was used to reduce hnRNP H2 protein levels in MCF-7 cells by 60–70% (Fig. 6*A*). After UV treatment, these cells were transfected with bicistronic mRNAs containing either the SHMT1 5′-UTR or the SHMT1 5′- and 3′-UTRs. Although hnRNP H2 depletion had no effect on the IRES activity of mRNA containing the 5′-UTR alone, the IRES activity of mRNA containing the 5′- and 3′-UTRs decreased 33% in UV- and hnRNP H2 siRNA-treated cells compared with UV-treated control cells (Fig. 6*B*). This reduction in IRES activity correlates with the decrease in SHMT1 protein levels observed upon hnRNP H2 knockdown in UV-treated cells (Fig. 6*A*).

In contrast to H ferritin and hnRNP H2, CUGBP1 protein levels decreased after UV exposure in the majority of the cell types tested (Fig. 3, *A–D*). However, given that CUGBP1 is primarily a nuclear protein under normal cellular conditions (36, 37), we hypothesized that CUGBP1 cellular localization changes, thereby enabling increased SHMT1 IRES activity after UV treatment. To test this hypothesis we determined the nuclear *versus* cytoplasmic distribution of CUGBP1 in MCF-7 cells by Western blot analysis (Fig. 7*A*) and immunofluorescence (Fig. 7*B*) 22 h after UV exposure. Both methods showed that CUGBP1 protein levels increase in the cytoplasm and decrease in the nucleus after UV treatment. CUGBP1 was also shown to be essential for IRES activation by UV. Treatment of MCF-7 cells with CUGBP1 siRNA depleted CUGBP1 protein levels by 90% compared with cells treated with negative control siRNA (Fig. 7*C*) and reduced SHMT1 protein levels (Fig. 7*C*) and IRES activity (Fig. 7*D*) in UV-treated cells by 50% compared with levels in cells treated with negative control siRNA. CUGBP1 depletion had the greatest impact on UV-activated IRES activity when the SHMT1 3′-UTR was present in the

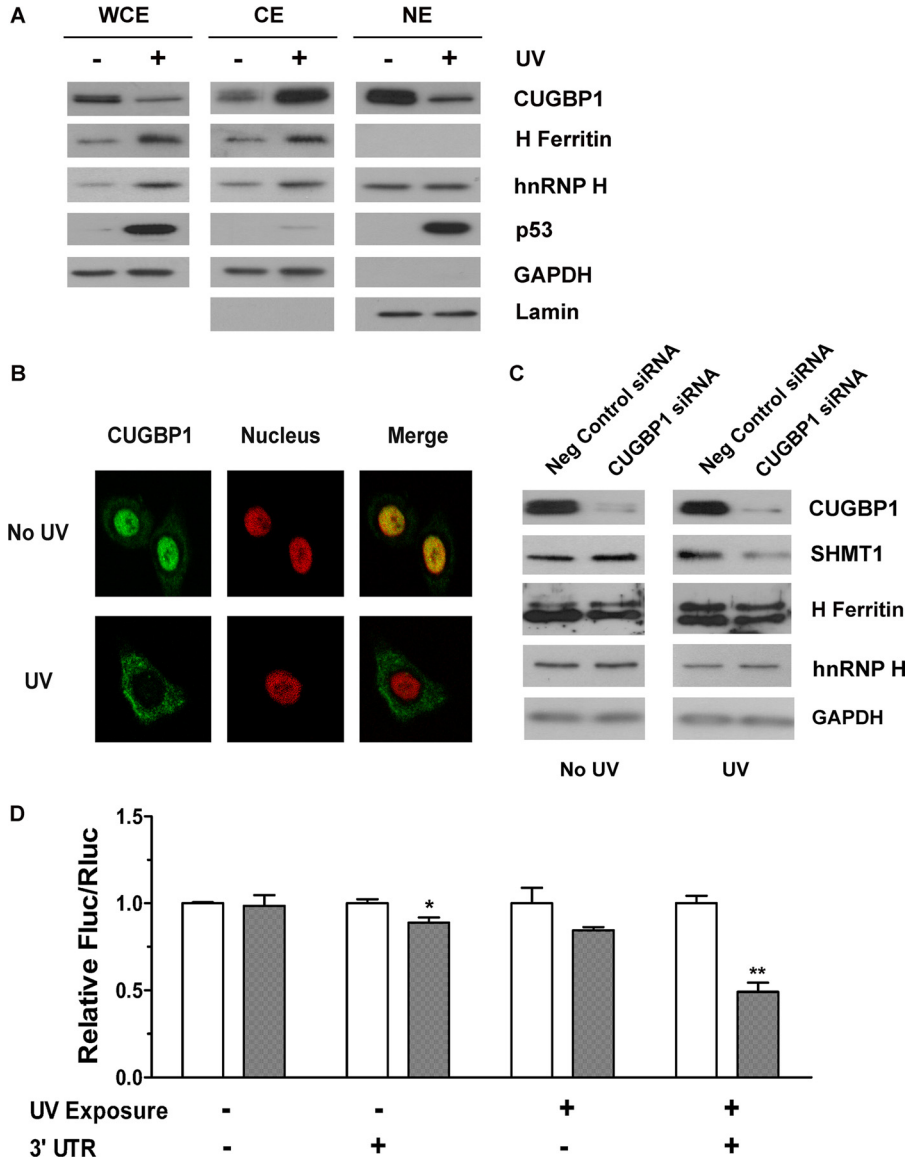

FIGURE 7. **Exposure to UV radiation results in the cytoplasmic accumulation of CUGBP1.** *A*, nuclear (*NE*) and cytoplasmic (*CE*) extracts were isolated from untreated and UV-treated MCF-7 cells 22 h after UV exposure. Whole cells extracts (*WCE*) were also obtained from the same samples. All extracts were run side-by-side on an SDS gel and subjected to immunoblotting using an anti-CUGBP1, anti-hnRNP H, or an anti-H ferritin antibody. p53 is shown as a control for UV treatment. GAPDH is shown as a control to demonstrate that the nuclear fractions are free of cytoplasmic contamination. Lamin A is shown as a control to demonstrate that the cytoplasmic fractions are free of nuclear contamination. Both GAPDH and Lamin A serve as controls for equal protein loading. *B*, immunofluorescence was used to determine CUGBP1 localization in untreated and UV-treated MCF-7 cells 22 h after UV exposure. CUGBP1 was visualized with Alexa Fluor 488 (*green*), and the nucleus was visualized with DRAQ5 (*red*). The *right column* is a merge of the green and red channels. *C*, MCF-7 cells were transfected with negative control siRNA or CUGBP1 siRNA and then treated with UV. 22 h after UV treatment, CUGBP1, SHMT1, hnRNP H, and H ferritin protein levels were visualized by Western blotting. GAPDH serves as a control for equal protein loading. *D*, the activity of the SHMT1 IRES was quantified as the Fluc/Rluc ratio in MCF-7 cells treated with negative control siRNA (*light bars*) and cells treated with CUGBP1 siRNA (*dark bars*). Cells were transfected with the bicistronic mRNA described in Fig. 5*A* containing or lacking the SHMT1 3′-UTR in the presence and absence of UVC exposure. For each experimental condition, values obtained from negative control siRNA-treated cells were given a relative value of 1.0. The data represent the average of three independent experiments ± S.E. The single and double *asterisks* represent statistical significance ($p = 0.04$ and $p = 0.002$, respectively) as determined by Student's *t* test.

bicistronic construct (Fig. 7*D*). Previously, we have shown that CUGBP1 exerts its effect on SHMT1 IRES activity by binding to the 3′-UTR of the transcript (26, 55). These data indicate that the increase in H ferritin and hnRNP H2 expression combined with the relocalization of CUGBP1 to the cytoplasm is responsible for the UV-mediated increase in SHMT1 IRES activity.

The Increase in SHMT1 Levels Is Independent of Cell Cycle—The increase in SHMT1 IRES activity could result directly from UV exposure or result from UV-induced inhibition of the cell cycle. Indeed, 24 h after UV exposure, MCF-7 cells exhibited cell cycle arrest in the G_2/M phase. Many cellular IRESs are known to be activated during G_2/M when cap-dependent translation is inhibited (38–40). To determine whether the enhanced levels of SHMT1 protein resulted directly from UV treatment or resulted from a UV-induced G_2/M cell cycle block, MCF-7 cells were treated with nocodazole, and changes in SHMT1 IRES activity, protein expression, and protein localization were monitored. Like UV, nocodazole arrests cells in the G_2/M phase of the cell cycle, but whereas UV acts by causing DNA damage, nocodazole acts by disrupting microtubules. After nocodazole treatment, 74% of the cells were arrested in the G_2/M phase of the cell cycle compared with 24% after UV treatment. However, nocodazole treatment did not affect SHMT1 IRES activity (Fig. 8*A*) or SHMT1, hnRNP H, or H ferritin protein levels (Fig. 8*B*). As in the case with UV treatment, CUGBP1 protein levels decreased in response to nocodazole treatment (Fig. 8*B*), but there was no relocalization from the nucleus to the cytoplasm (Fig. 8*C*). These results demonstrate that the increase in SHMT1 levels after UV treatment was not the result of cell cycle arrest at G_2/M and raised the possibility that SHMT1, through its involvement in *de novo* thymidylate biosynthesis, plays a role in NER.

SHMT1 Enhances Genome Stability after UV Exposure—To test the hypothesis that SHMT1 is involved in the repair of UV-induced DNA damage, we determined the impact of SHMT1 depletion (Fig. 9*A*) on genome stability after UV treatment using the comet assay. The assay involves the use of electrophoresis to separate intact DNA from damaged DNA, which forms a "comet" (Fig. 9*B*). The head of the comet represents intact DNA, and DNA-containing strand breaks comprises the comet tail. Four different parameters

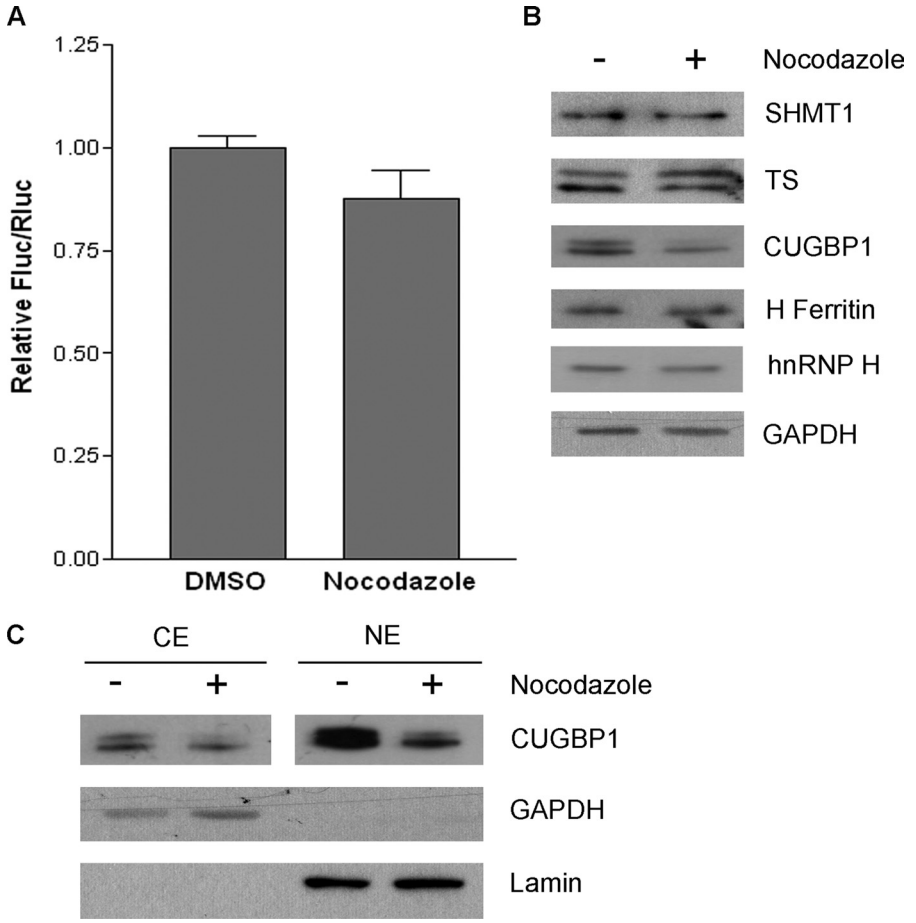

FIGURE 8. **Nocodazole treatment does not produce the same effects as UV radiation.** *A*, MCF-7 cells were treated with either vehicle (DMSO) or 60 ng/ml nocodazole for 24 h and then transiently transfected with the bicistronic mRNA in Fig. 5*A*. The ratio of Fluc/Rluc in DMSO-treated cells was given a value of 1.0. The data represent the average of three independent experiments ±S.E. *B*, total protein lysates were prepared from untreated and nocodazole-treated cells and resolved by SDS-PAGE. Protein levels were determined by immunoblotting using antibodies against SHMT1, TS, CUGBP1, and H ferritin. GAPDH served as a control for equal protein loading. *C*, nuclear (*NE*) and cytoplasmic (*CE*) fractions were also isolated from these cells and subjected to immunoblotting using an anti-CUGBP1 antibody. GAPDH is shown as a control to demonstrate that the nuclear fractions are free of cytoplasmic contamination. Lamin A is shown as a control to demonstrate that the cytoplasmic fractions are free of nuclear contamination. Both GAPDH and Lamin A serve as controls for equal protein loading.

were calculated for each comet as defined under "Experimental Procedures": % tail DNA, extent tail moment, olive tail moment, and tail length. All parameters are directly proportional to the amount of DNA strand breaks. Before UV treatment, SHMT1 depletion did not affect any of the comet assay parameters, indicating that SHMT1 did not influence DNA integrity before UV exposure. After UV exposure, SHMT1 depletion resulted in increased levels of DNA damage compared with the control cells for each comet assay parameter measured (Fig. 9, *C–F*). The increased amount of DNA damage in the SHMT1-depleted cells correlates with the reduced viability of these cells relative to control cells after UV treatment (Fig. 9*G*) and supports a role for SHMT1 in the repair of UV-induced DNA damage.

SHMT1 and TS Localize to the Nucleus in Response to UV Treatment—De novo thymidylate biosynthesis occurs in both the cytoplasm and the nucleus (Fig. 1). Nuclear thymidylate biosynthesis is enabled by the SUMO-dependent nuclear import of SHMT1 and TS (12, 13). An increase in SUMOylation in response to UV treatment has previously been reported for several proteins involved in cellular stress response including TIP60 (41), xeroderma pigmentosum, complementation group C (42), and DJ-1 (43). Immunoprecipitation of SHMT1 and TS from untreated and UV-treated MCF-7 whole cell extract revealed that the SUMOylation of these proteins is likewise increased in response to UV radiation (Fig. 10, *A* and *B*). These findings are supported by an increase in the amount of SHMT1 and TS in the nucleus of UV-treated cells (Fig. 10*C*). In the case of TS, increased nuclear concentration occurs despite an overall decrease in protein levels (Figs. 3*A* and 10*C*).

DISCUSSION

The results from this study demonstrate a role for SHMT1 and nuclear folate-dependent thymidylate biosynthesis in the repair of UV-induced DNA damage. Previous studies have demonstrated that SHMT1 activity is the rate-limiting activity in thymidylate biosynthesis in MCF-7 cells. Overexpression of SHMT1 in MCF-7 cells not only favors the partitioning of folate-derived one-carbon units to thymidylate biosynthesis but also enhances the efficiency of *de novo* thymidylate biosynthesis relative to synthesis through the salvage pathway (11). Unlike the other enzymes involved in folate-mediated one-carbon metabolism, SHMT1 expression is not ubiquitous. Although it is expressed primarily in the liver and kidney (44), significant amounts of the SHMT1 transcript are present in exposed tissues of the body such as the eyes and skin (UniGene, National Center for Biotechnology Information; Fig. 3*C*), which are highly susceptible to UV-induced DNA damage.

The UV-responsive IRES located within the 5′-UTR of the SHMT1 transcript enables SHMT1 to escape the control mechanisms that repress cap-dependent translation during cellular stress and to function in DNA repair. SHMT1 is not the only protein whose expression is activated by a UV-responsive IRES. It was recently shown that lethal doses of UVC result in an increase in both the IRES activity and protein levels of the pro-apoptotic factor Apaf-1 (23). However, this is the first report to our knowledge of a UV-responsive IRES that regulates the translation of a protein involved in DNA repair. Whereas the mechanism responsible for the UV-induced activation of the Apaf-1 IRES has yet to be

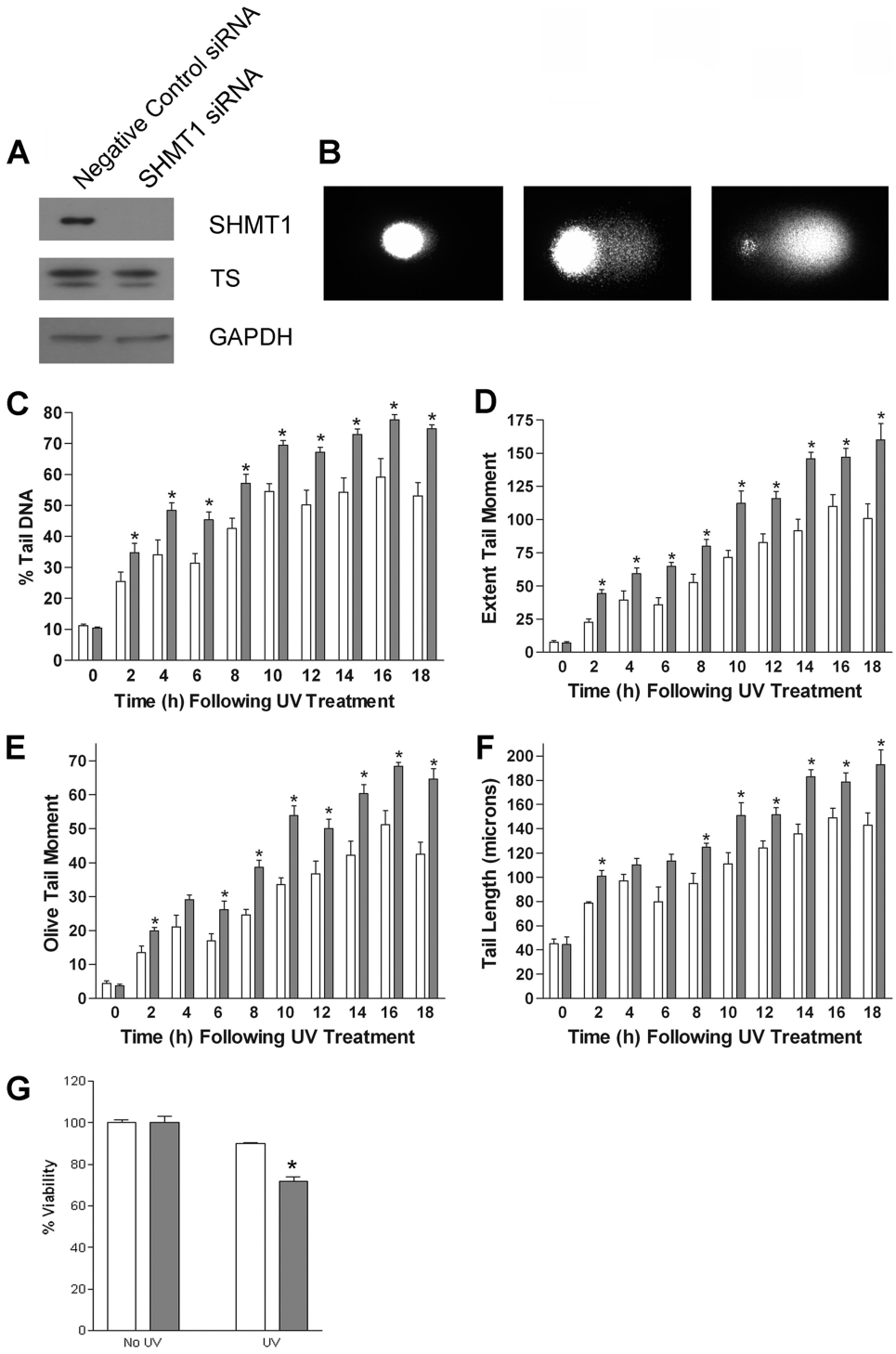

FIGURE 9. **SHMT1 is involved in the repair of UV-induced DNA damage.** MCF-7 cells were treated with negative control siRNA (*light bars*) or SHMT1 siRNA (*dark bars*) for 55 h and then exposed to UV radiation. At the indicated times after UV treatment, the cells were harvested and divided into two samples. One sample was used for immunoblotting to ensure the knockdown of SHMT1, and the other sample was used in the comet assay to determine DNA damage or in the MTT assay to determine cell viability. *A*, shown is a representative Western blot showing SHMT1 and TS protein levels in cells treated with either the negative control siRNA or the SHMT1 siRNA. GAPDH serves as a control for equal protein loading. *B*, for the comet assay, single cells were embedded in agarose, lysed, and subjected to electrophoresis. The DNA content of each cell was visualized using SYBR Gold. The panels are representative images of (from *left* to *right*) a cell with little DNA damage, a cell with an intermediate amount of DNA damage, and a cell with extensive DNA damage. *C–F*, the DNA content of the cells was quantified using Komet 5.5 software. The data represent the average of three independent experiments ±S.E. Each experiment was performed in duplicate, and 75 cells were analyzed per experiment per time point. The *asterisk* represents statistical significance ($p < 0.05$) at a given time point as determined by Student's *t* test. *C*, % tail DNA = the proportion of DNA that has migrated from the nucleoid core. *D*, extent of tail moment = % tail DNA × tail length/100. *E*, olive tail moment = (tail center of gravity − head center of gravity) × % tail DNA/100. *F*, tail length = the distance (microns) of DNA migration from the nucleoid core. *G*, for the MTT assay, the production of formazan by living mitochondria was measured in negative control siRNA-treated cells (*light bars*) and SHMT1 siRNA-treated cells (*dark bars*) 24 h after UV treatment by recording the absorbance at 550 nm. The absorbance from non-irradiated, negative control siRNA-treated cells was given a value of 100%. The results represent the average of four independent experiments ±S.E. The *asterisk* indicates statistical significance ($p = 0.0002$) as determined by Student's *t* test.

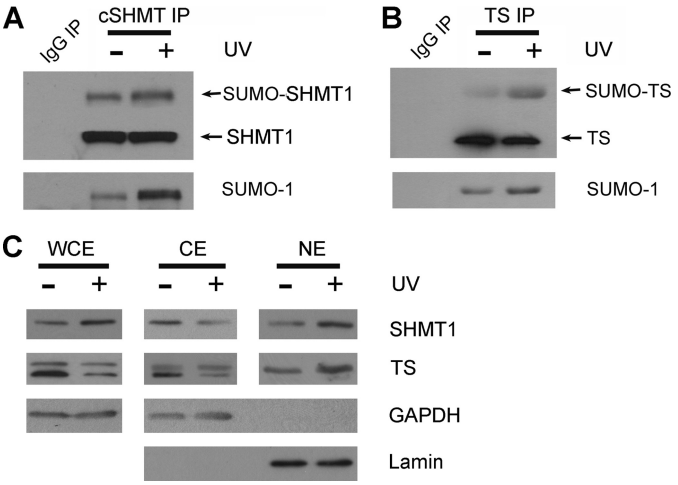

FIGURE 10. **SHMT1 and TS SUMOylation and nuclear localization increase in response to UV treatment.** SHMT1 (*A*) and TS (*B*) were immunoprecipitated (*IP*) from untreated and UV-treated MCF-7 whole cell extracts 22 h after UV exposure. Immunoblotting was performed on the immunoprecipitates using antibodies against SUMO-1, SHMT1, and TS. The IgG immunoprecipitate (*lane 1*) serves as control for nonspecific binding. *C*, whole cell (*WCE*), nuclear (NE), and cytoplasmic (*CE*) fractions were isolated from untreated and UV-treated MCF-7 cells 22 h after UV exposure. All extracts were resolved by SDS-PAGE and subjected to immunoblotting using an anti-SHMT1 or anti-TS antibody. GAPDH is shown as a control to demonstrate that the nuclear fractions are free of cytoplasmic contamination. Lamin A is shown as a control to demonstrate that the cytoplasmic fractions are free of nuclear contamination. Both GAPDH and Lamin A serve as controls for equal protein loading.

determined, we have shown that changes in the concentration of H ferritin and hnRNP H2 and a change in the localization of CUGBP1 enables the UV-induced IRES-mediated translation of SHMT1.

H ferritin has previously been proposed to play an important role in protecting cells from UV-induced DNA damage. By sequestering free iron, it prevents the conversion of UV-generated reactive oxygen species to even more damaging hydroxyl radicals via the Fenton reaction (45, 46). Based on the results of this study, we can now ascribe an additional role to H ferritin in the DNA damage response, as it increases SHMT1 expression for NER by stimulating the IRES-mediated translation of SHMT1.

The mechanisms by which hnRNP H2 protein levels increase and CUGBP1 relocalizes to the cytoplasm after UV treatment remain to be determined. Because global protein synthesis decreases upon UV exposure and because hnRNP H2 mRNA is not known to contain an IRES, changes in transcription or protein stability most likely contribute to the accumulation of hnRNP H2. Several studies have shown that changes in the phosphorylation status of a protein can alter its cellular localization (47–50). As it is known that CUGBP1 is phosphorylated *in vivo* (51), it is interesting to speculate that a UV-responsive kinase is responsible for the translocation of CUGBP1 from the nucleus to the cytoplasm.

The involvement of SHMT1 in DNA repair is supported by the increase in SHMT1 and TS SUMOylation and nuclear compartmentation in response to UV radiation. Nuclear SHMT1 and TS form a complex with proliferating cell nuclear antigen, the processivity factor for the NER polymerase.[3] Although thymidylate generated in the cytoplasm can freely diffuse into the nucleus, production of this deoxyribonucleotide directly at the site of DNA repair may allow for more rapid DNA synthesis and enhance the fidelity of the repair polymerase by decreasing uracil misincorporation. As uracil misincorporation can ultimately result in DNA strand breaks (4), this would account for the decrease in DNA damage observed in UV-treated control cells compared with those depleted of SHMT1 (Fig. 8, *C–F*).

In mice such a response to UV-induced DNA damage is not possible as the 5′-UTR of the murine SHMT1 transcript, which shares only 42% sequence identity with the human SHMT1 5′-UTR, lacks IRES activity (26). The species specificity of the UV-inducible SHMT1 IRES suggests that it may have evolved as an adaptive response to protect the skin from UV damage.

[3] P. J. Stover and D. D. Anderson, unpublished results.

REFERENCES

1. Ravanat, J. L., Douki, T., and Cadet, J. (2001) *J. Photochem. Photobiol. B* **63,** 88–102
2. Tornaletti, S., and Hanawalt, P. C. (1999) *Biochimie* **81,** 139–146
3. de Laat, W. L., Jaspers, N. G., and Hoeijmakers, J. H. (1999) *Genes Dev.* **13,** 768–785
4. Hori, T., Ayusawa, D., Shimizu, K., Koyama, H., and Seno, T. (1984) *Cancer Res.* **44,** 703–709
5. Scott, J. M., and Weir, D. G. (1981) *Lancet* **2,** 337–340
6. Suh, J. R., Herbig, A. K., and Stover, P. J. (2001) *Annu. Rev. Nutr.* **21,** 255–282
7. Schirch, V., and Strong, W. B. (1989) *Arch. Biochem. Biophys.* **269,** 371–380
8. Strong, W. B., Tendler, S. J., Seither, R. L., Goldman, I. D., and Schirch, V. (1990) *J. Biol. Chem.* **265,** 12149–12155
9. Reed, M. C., Nijhout, H. F., Neuhouser, M. L., Gregory, J. F., 3rd, Shane, B., James, S. J., Boynton, A., and Ulrich, C. M. (2006) *J. Nutr.* **136,** 2653–2661
10. Green, J. M., MacKenzie, R. E., and Matthews, R. G. (1988) *Biochemistry* **27,** 8014–8022
11. Herbig, K., Chiang, E. P., Lee, L. R., Hills, J., Shane, B., and Stover, P. J. (2002) *J. Biol. Chem.* **277,** 38381–38389
12. Woeller, C. F., Anderson, D. D., Szebenyi, D. M., and Stover, P. J. (2007) *J. Biol. Chem.* **282,** 17623–17631
13. Anderson, D. D., Woeller, C. F., and Stover, P. J. (2007) *Clin. Chem. Lab. Med.* **45,** 1760–1763
14. Anderson, D. D., and Stover, P. J. (2009) *PLoS One* **4,** e5839
15. Laiho, M., and Latonen, L. (2003) *Ann. Med.* **35,** 391–397
16. Fritz, G., and Kaina, B. (1999) *Mol. Cell. Biol.* **19,** 1768–1774
17. Bender, K., Blattner, C., Knebel, A., Iordanov, M., Herrlich, P., and Rahmsdorf, H. J. (1997) *J. Photochem. Photobiol. B* **37,** 1–17
18. Deng, J., Harding, H. P., Raught, B., Gingras, A. C., Berlanga, J. J., Scheuner, D., Kaufman, R. J., Ron, D., and Sonenberg, N. (2002) *Curr. Biol.* **12,** 1279–1286
19. Jiang, H. Y., and Wek, R. C. (2005) *Biochem. J.* **385,** 371–380
20. Wu, S., Hu, Y., Wang, J. L., Chatterjee, M., Shi, Y., and Kaufman, R. J. (2002) *J. Biol. Chem.* **277,** 18077–18083
21. Gebauer, F., and Hentze, M. W. (2004) *Nat. Rev. Mol. Cell Biol.* **5,** 827–835
22. Mazan-Mamczarz, K., Galbán, S., López de Silanes, I., Martindale, J. L., Atasoy, U., Keene, J. D., and Gorospe, M. (2003) *Proc. Natl. Acad. Sci. U.S.A.* **100,** 8354–8359
23. Ungureanu, N. H., Cloutier, M., Lewis, S. M., de Silva, N., Blais, J. D., Bell, J. C., and Holcik, M. (2006) *J. Biol. Chem.* **281,** 15155–15163
24. Holcik, M., Sonenberg, N., and Korneluk, R. G. (2000) *Trends Genet.* **16,** 469–473
25. Spriggs, K. A., Stoneley, M., Bushell, M., and Willis, A. E. (2008) *Biol. Cell* **100,** 27–38
26. Woeller, C. F., Fox, J. T., Perry, C., and Stover, P. J. (2007) *J. Biol. Chem.* **282,** 29927–29935
27. Bensadoun, A., and Weinstein, D. (1976) *Anal. Biochem.* **70,** 241–250
28. Oppenheim, E. W., Adelman, C., Liu, X., and Stover, P. J. (2001) *J. Biol.*

Chem. **276,** 19855–19861
29. MacFarlane, A. J., Liu, X., Perry, C. A., Flodby, P., Allen, R. H., Stabler, S. P., and Stover, P. J. (2008) *J. Biol. Chem.* **283,** 25846–25853
30. Shieh, S. Y., Ikeda, M., Taya, Y., and Prives, C. (1997) *Cell* **91,** 325–334
31. Bushell, M., Stoneley, M., Kong, Y. W., Hamilton, T. L., Spriggs, K. A., Dobbyn, H. C., Qin, X., Sarnow, P., and Willis, A. E. (2006) *Mol. Cell* **23,** 401–412
32. Dobbyn, H. C., Hill, K., Hamilton, T. L., Spriggs, K. A., Pickering, B. M., Coldwell, M. J., de Moor, C. H., Bushell, M., and Willis, A. E. (2008) *Oncogene* **27,** 1167–1174
33. Lewis, S. M., Veyrier, A., Hosszu Ungureanu, N., Bonnal, S., Vagner, S., and Holcik, M. (2007) *Mol. Biol. Cell* **18,** 1302–1311
34. Legrand-Poels, S., Schoonbroodt, S., Matroule, J. Y., and Piette, J. (1998) *J. Photochem. Photobiol. B* **45,** 1–8
35. Pham, C. G., Bubici, C., Zazzeroni, F., Papa, S., Jones, J., Alvarez, K., Jayawardena, S., De Smaele, E., Cong, R., Beaumont, C., Torti, F. M., Torti, S. V., and Franzoso, G. (2004) *Cell* **119,** 529–542
36. Timchenko, L. T., Miller, J. W., Timchenko, N. A., DeVore, D. R., Datar, K. V., Lin, L., Roberts, R., Caskey, C. T., and Swanson, M. S. (1996) *Nucleic Acids Res.* **24,** 4407–4414
37. Michalowski, S., Miller, J. W., Urbinati, C. R., Paliouras, M., Swanson, M. S., and Griffith, J. (1999) *Nucleic Acids Res.* **27,** 3534–3542
38. Cormier, P., Pyronnet, S., Salaün, P., Mulner-Lorillon, O., and Sonenberg, N. (2003) *Prog. Cell Cycle Res.* **5,** 469–475
39. Pyronnet, S., and Sonenberg, N. (2001) *Curr. Opin. Genet. Dev.* **11,** 13–18
40. Sachs, A. B. (2000) *Cell* **101,** 243–245
41. Cheng, Z., Ke, Y., Ding, X., Wang, F., Wang, H., Wang, W., Ahmed, K., Liu, Z., Xu, Y., Aikhionbare, F., Yan, H., Liu, J., Xue, Y., Yu, J., Powell, M., Liang, S., Wu, Q., Reddy, S. E., Hu, R., Huang, H., Jin, C., and Yao, X. (2008) *Oncogene* **27,** 931–941
42. Wang, Q. E., Zhu, Q., Wani, G., El-Mahdy, M. A., Li, J., and Wani, A. A. (2005) *Nucleic Acids Res.* **33,** 4023–4034
43. Shinbo, Y., Niki, T., Taira, T., Ooe, H., Takahashi-Niki, K., Maita, C., Seino, C., Iguchi-Ariga, S. M., and Ariga, H. (2006) *Cell Death Differ.* **13,** 96–108
44. Girgis, S., Nasrallah, I. M., Suh, J. R., Oppenheim, E., Zanetti, K. A., Mastri, M. G., and Stover, P. J. (1998) *Gene* **210,** 315–324
45. Balla, G., Jacob, H. S., Balla, J., Rosenberg, M., Nath, K., Apple, F., Eaton, J. W., and Vercellotti, G. M. (1992) *J. Biol. Chem.* **267,** 18148–18153
46. Stohs, S. J., and Bagchi, D. (1995) *Free Radic. Biol. Med.* **18,** 321–336
47. Habelhah, H., Shah, K., Huang, L., Ostareck-Lederer, A., Burlingame, A. L., Shokat, K. M., Hentze, M. W., and Ronai, Z. (2001) *Nat. Cell Biol.* **3,** 325–330
48. Xie, J., Lee, J. A., Kress, T. L., Mowry, K. L., and Black, D. L. (2003) *Proc. Natl. Acad. Sci. U.S.A.* **100,** 8776–8781
49. Zhou, B. P., Liao, Y., Xia, W., Spohn, B., Lee, M. H., and Hung, M. C. (2001) *Nat. Cell Biol.* **3,** 245–252
50. van der Houven, van Oordt, W., Diaz-Meco, M. T., Lozano, J., Krainer, A. R., Moscat, J., and Cáceres, J. F. (2000) *J. Cell Biol.* **149,** 307–316
51. Timchenko, N. A., Wang, G. L., and Timchenko, L. T. (2005) *J. Biol. Chem.* **280,** 20549–20557
52. Harding, H. P., Zhang, Y., Zeng, H., Novoa, I., Lu, P. D., Calfon, M., Sadri, N., Yun, C., Popko, B., Paules, R., Stojdl, D. F., Bell, J. C., Hettmann, T., Leiden, J. M., and Ron, D. (2003) *Mol. Cell* **11,** 619–633
53. Harding, H. P., Novoa, I., Zhang, Y., Zeng, H., Wek, R., Schapira, M., and Ron, D. (2000) *Mol. Cell* **6,** 1099–1108
54. Vattem, K. M., and Wek, R. C. (2004) *Proc. Natl. Acad. Sci. U.S.A.* **101,** 11269–11274
55. Fox, J. T., and Stover, P. J. (2009) *J. Biol. Chem.*, **284,** 31085–31096